



## ORIGINAL PAPER

**EFFECTS OF STRENGTH WEAKENING AND INTERFACE SLIPPING ON ROCK MASS WITH DIFFERENT DIP ANGLE STRUCTURE PLANES****Pu WANG<sup>1,2)\*</sup>, Lishuai JIANG<sup>3)</sup>, Xiaoyu LI<sup>3)</sup>, Pengqiang ZHENG<sup>1,2)</sup> and Guangpeng QIN<sup>1,2)\*</sup>**<sup>1)</sup>Department of Resources and Civil Engineering, Shandong University of Science and Technology, Tai'an, 271019, China<sup>2)</sup>National Engineering Laboratory for Coalmine Backfilling Mining, Shandong University of Science and Technology, Tai'an, 271019, China<sup>3)</sup>State Key Laboratory of Mining Disaster Prevention and Control Co-founded by Shandong Province and the Ministry of Science and Technology, Shandong University of Science and Technology, Qingdao 266590, China

\*Corresponding author's e-mail: 15854848872@163.com; friendqgp@163.com

**ARTICLE INFO****Article history:**

Received 27 August 2018

Accepted 12 October 2018

Available online 18 October 2018

**Keywords:**

Structure plane

Different dip angle

Strength weakening effect

Interface slipping effect

Rock burst

**ABSTRACT**

Micro-mechanical behaviors of rock masses with structure planes can provide information regarding precursory characteristics of macro-fracture of strata and rock bursts. Hence, numerical simulation with uniaxial compression test is conducted using Realistic Failure Process Analysis (RFPA). Then, mechanical properties and progressive failure processes for rock masses with different dip angle structure planes are studied, and the macroscopic fractures, mechanical responses, and acoustic emission (AE) responses of rock masses are analyzed. Moreover, the strength weakening and interface slipping effects with different dip angle structure planes are revealed. The results show that rocks with different dip angle structure planes show significant strength and interface slipping effects. A small dip angle structure plane has little influence on the rock strength and interface slipping, which mainly manifests as failure in rock interiors. For medium dip angle structure plane, the rock strength decreases obviously, and interface slipping is notable along the structure plane. The effects caused by the weak plane are more prominent with rising dip angles. Compared to rocks with small dip angle structure planes, those with medium dip angle structure planes are more easily broken. However, the total energy released and total AE counts are smaller, indicating less serious bursting liability from rock failure.

**1. INTRODUCTION**

Because of the joints, cracks, or faults that universally occur in natural rock masses, the strength effect on their mechanical properties is notable. Specifically, when a fault occurs, the rock masses on two fault walls may slip along the fault plane, which can instantaneously release a large amount of elastic strain energy, thereby inducing serious dynamic disasters (i.e., rock bursts, shock bumps) (Jiang et al., 2018; Jiang et al., 2017). Figure 1 depicts several field images of the sites after accidents. This indicates that a rock burst caused by fault occurrence is closely related to the strength and interface slipping effects of the rock mass. Moreover, the aforementioned structure surfaces can show significant discontinuity and inhomogeneity for the rocks, which also has notable effect on rock bursts (Tang et al., 2010).

Regarding the structure plane mechanical properties for a rock mass, laboratory tests (Cao et al., 2018; Lee et al., 2017; Day et al., 2017; Feng et al., 2017; Moayed et al., 2016; Jiang et al., 2013) or numerical simulations (Bahaaddini et al., 2017; Wang et al., 2017; Kim et al., 2016; Bahaaddini et al.,

2016; Cao et al., 2015) were commonly performed, including tests of direct shear and triaxial stress, and bi-directional and double-sided shear friction (Wang, 2012), as shown in Figure 2. However, laboratory tests have the disadvantage of tedious production and heavy work. For instance, usually a drilling machine is required to retrieve the specimens and polish them; then, the specimens must be handled according to the test scheme. Moreover, the theoretical calculations do not accurately and intuitively reflect the characteristics of macroscopic rupture, mechanical responses, and acoustic emission (AE) responses.

Therefore, in this paper, according to the study targets and considering the heterogeneity of rock material, a numerical simulation with uniaxial compression test using Realistic Failure Process Analysis (RFPA), which obeys Weibull distribution and is usually used to effectively consider the inhomogeneity of a brittle material, is conducted. Then, mechanical properties and progressive failure processes for rock masses with different dip angle structure planes are studied, and the macroscopic fracture, mechanical responses, and AE responses of



Fig. 1 Field images of sites captured after accidents.

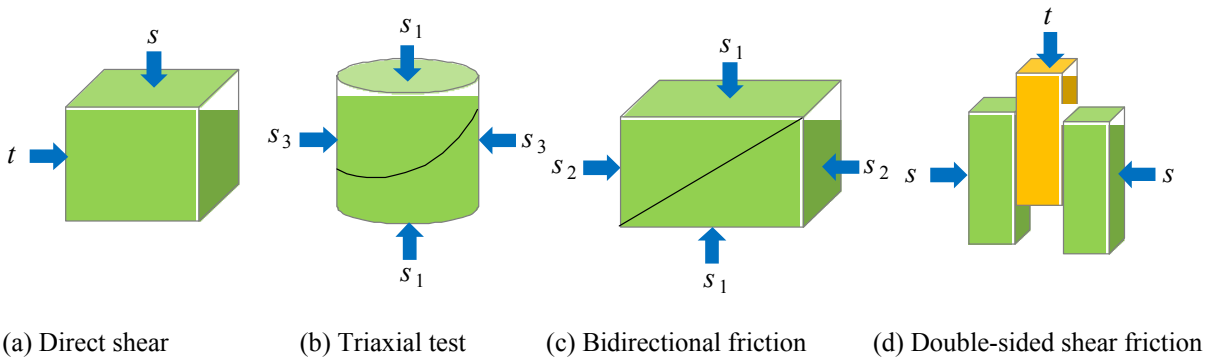


Fig. 2 Study methods of mechanical properties for rock mass structure plane (Reproduced with permission from Wang T. 2012, Mechanism of coal bumps induced by fault reactivation. Ph.D. thesis, China University of Mining and Technology, Beijing, China).

rock masses are analyzed. Moreover, the strength weakening and interface slipping effects with different dip angle structure planes are revealed. The results presented here form a solid foundation for the study of rock bursts in the vicinity of faults.

2. MECHANICAL EFFECT OF FAULT PLANE

Figure 3 depicts a fault which is described by Anderson (Cai, 2015). A mechanical model is established and analyzed by choosing a microunit from a fault plane. The length of AB as  $l$ , the normal stress, and shear stress of fault plane in the Cartesian coordinate system can be expressed based on the mechanical equilibrium, as shown in Eq. (1).

$$\begin{cases} \sigma_n = \frac{\sigma_1 + \sigma_3}{2} + \frac{\sigma_1 - \sigma_3}{2} \cos 2\alpha \\ \tau_n = \frac{\sigma_1 - \sigma_3}{2} \sin 2\alpha \end{cases} \quad (1)$$

where  $\sigma_n$  and  $\tau_n$  are the normal and shear stresses of the fault plane, respectively, MPa;  $\sigma_1$  and  $\sigma_3$  are the maximum and minimum principal stresses, MPa;  $\alpha$  is the fault dip angle measured in degrees ( $^\circ$ ).

When a rock mass with a structural plane is destroyed along the weak plane, the shear stress acting on the plane ( $\tau_n$ ) should exceed its ultimate shear stress ( $\tau_f$ ) caused by the normal stress. Hence, the critical condition of rock slipping along the weak plane can be shown in Eq. (2) based on the relation  $\tau_f = \tau_n$ .

$$\sigma_1 - \sigma_3 = \frac{2(\sigma_3 \cdot \tan \varphi_f + c)}{(1 - \tan \varphi_f \cdot \cot \alpha) \sin 2\alpha} \quad (2)$$

where  $\tau_f$  is the ultimate shear stress caused by the normal stress, MPa. It satisfies the Mohr–Coulomb strength criterion and can be expressed by  $\tau_f = \sigma_n \tan \varphi_f + c_f$  (Hubbert and Rubey, 1961).  $\varphi_f$  is the internal friction angle of the fault plane, in degrees, and  $c_f$  is the cohesive strength of the fault plane, MPa.

From Eq. (2), when  $\alpha = 90^\circ$  or  $\alpha \rightarrow \varphi_f$ , the expression  $(\sigma_1 - \sigma_3) \rightarrow \infty$  is established. Hence, the range of fault dip angles for rock breaks along the fault planes are given by Eq. (3) (Shen and Chen, 2006).

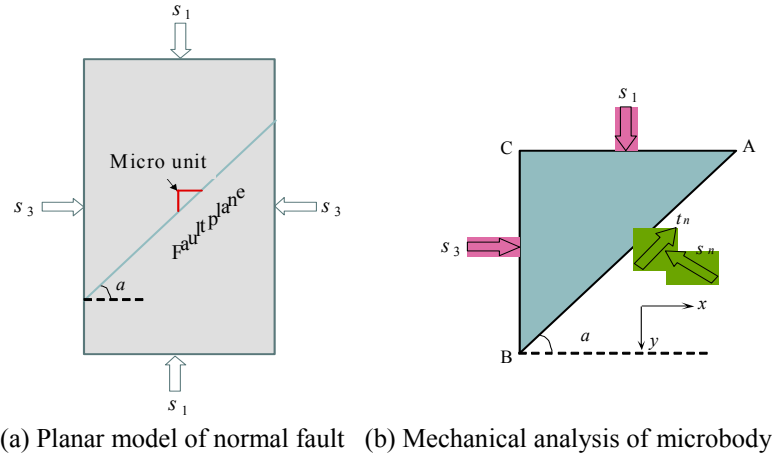


**Fig. 3** Mechanical model of fault.

$$\varphi_f < \alpha < 90^\circ \quad (3)$$

The relationship between the fault dip angle and its internal friction angle is obtained by finding the first derivative of  $\alpha$  and equating to zero. Thus, Eq. (4) is given as follows.

$$\alpha = \frac{\varphi_f}{2} + 45^\circ \quad (4)$$

The critical condition of rock failure along the fault plane (i.e., fault slipping) is obtained as shown in Eq. (5), by substituting Eq. (4) into Eq. (2).

$$(\sigma_1 - \sigma_3)_{\min} = 2(\sigma_3 \cdot \tan \varphi_f + c) \cdot \frac{1 - \sin \varphi_f}{\cos \varphi_f} \quad (5)$$

From Eqs. (4) and (5), we can see that the critical condition of rock failure along a fault plane is related to the fault dip angle  $\alpha$  and the confining pressure  $\sigma_3$ . Hence, to intuitively study the problem, Eq. (5) is solved by selecting  $\varphi_f = 30^\circ$  and  $c = 0.4$  MPa (Sainoki and Mitri, 2014). Figure 4 shows the relationship among fault-slipping, fault dip angle ( $\alpha$ ), and confining stress ( $\sigma_3$ ).

As shown in Figure 4, regardless of the magnitude of confining pressure applied, the curves are symmetrical about the straight line  $\alpha = \frac{\varphi_f}{2} + 45^\circ$  in the range of  $(\varphi_f, 90)$ ; moreover, the minimum value of the principal stress difference is at the point  $\alpha = \frac{\varphi_f}{2} + 45^\circ$ , which indicates that it is most likely to slip along the fault plane. When the fault dip angle is close to  $\varphi_f$  or  $90^\circ$ , the principal stress difference tends to infinity; however, if it reaches or exceeds its corresponding ultimate failure strength, the rock will no longer slip along the fault plane, but will be destroyed from inside.

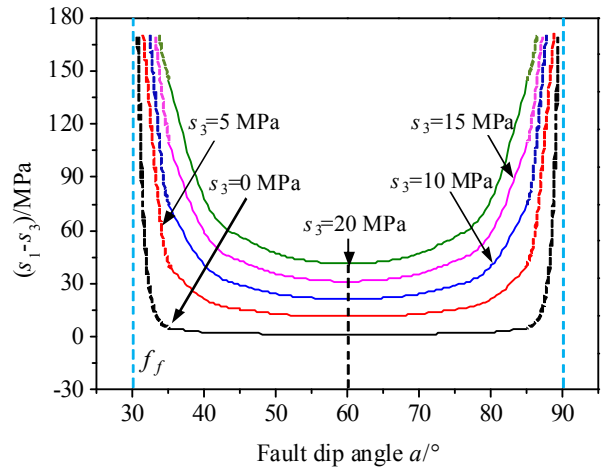


**Fig. 4** Relationship among fault-slipping, fault dip angle ( $\alpha$ ), and confining stress ( $\sigma_3$ ).

### 3. NUMERICAL ANALYSIS OF EFFECTS ON STRENGTH AND INTERFACE SLIPPING FOR ROCK MASS

#### 3.1. ESTABLISHMENT OF RFPA MODEL

Considering the rock heterogeneity, rock models with different dip angle structure planes are established using RFPA numerical software. According to the analysis in Section 2, regardless of the amount of confining pressure applied, the relationship between fault slipping and fault dip angle is consistent; hence, in this section, the relationship with no confining pressure (i.e.,  $\sigma_3 = 0$  MPa) is chosen and studied. Then, the macroscopic fracture appearance, mechanical responses, and AE responses of the rock specimen are simulated and analyzed by the uniaxial compression displacement loading method.

The lithology of rock specimen is selected as sandstone, and the preset structure plane is in the middle of the specimen, running through the whole rock. The size of the specimen is designed to be

**Table 1** Mechanical parameters of coal and rocks (Zhao et al., 2013).

| Media Type      | Modulus of elasticity (MPa) | Average strength (MPa) | Poisson ratio | Homogeneity index |
|-----------------|-----------------------------|------------------------|---------------|-------------------|
| Sandstone       | 13500                       | 40                     | 0.22          | 2.5               |
| Structure plane | 2000                        | 18                     | 0.3           | 2                 |

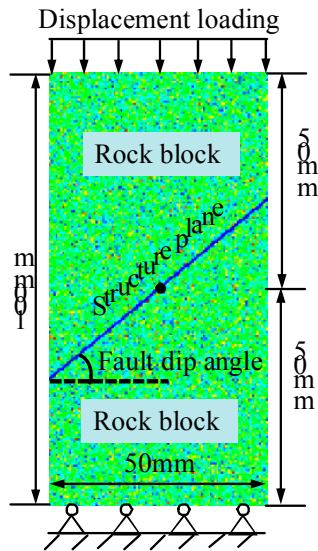


**Fig. 5** Calculation model of RFPA.

50 mm (width) × 100 mm (height), and the division units are 50 × 100=5000. Considering the symmetry analysis of fault slipping in section 2 and the model sizes, the dip angle of structure plane is preset to 10°, 20°, 30°, 40°, 50°, and 60°, and its width is set to 1 mm. The model calculation adopts the plane stress model and uniaxial compression axial displacement loading. Figure 5 shows the calculation model of RFPA. The initial displacement value applied on the model sets to 0.002 mm, and the displacement increment at each loading-step is 0.003 mm, until it is destroyed. The mechanical parameters of the meso unit of the rock are shown in Table 1 (Zhao et al., 2013; Ma et al., 2007).

**3.2. RESULTS OF RFPA SIMULATION**

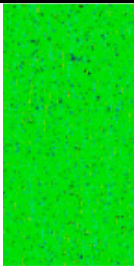
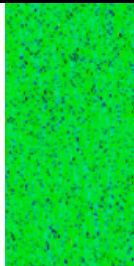
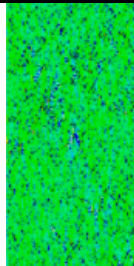
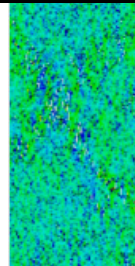
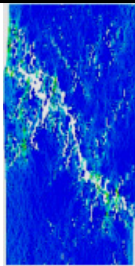
**3.2.1. FAILURE PROCESS OF ROCK MASS WITH DIFFERENT DIP ANGLE STRUCTURE PLANES**

The uniaxial compression tests of rock specimens with different dip angle structure planes and the intact specimen without a preset structure plane in Figure 5 are carried out. The failure process of the specimens is shown in Tables 2–4. The failure patterns of rock specimens with different dip angle structure planes are different.

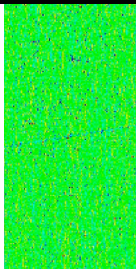
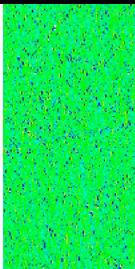
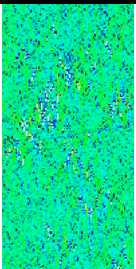
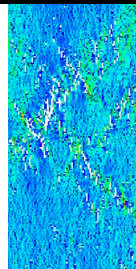
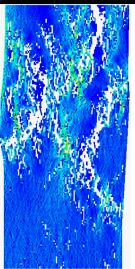
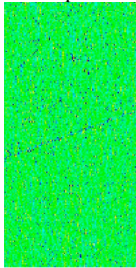
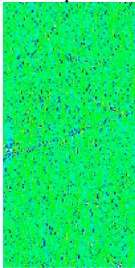
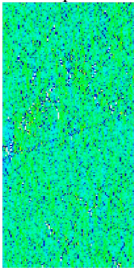
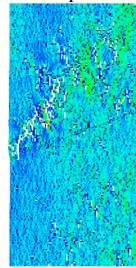
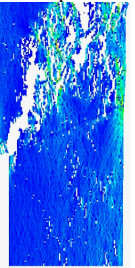
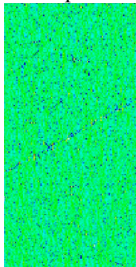
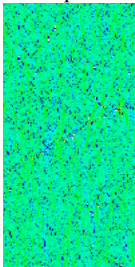
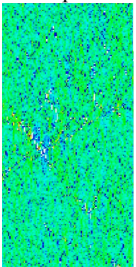
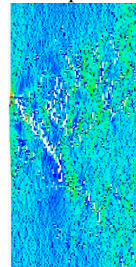
As shown in Table 2, regarding the intact rock specimen, at the 20th step, the upper part of the specimen presents obvious instability units, while the lower part is relatively unobvious. At 31 steps, the number of instability units rises notably and with a random distribution; moreover, they spread throughout the whole rock, but no cracks are formed. At the 37th step, the instability units continue to increase and interconnect, and then many local microcracks occur. At the 40th step, microcracks expand significantly, while the concentrated stress at the crack tip further causes the crack to expand, thereby interconnecting and forming an obvious macroscopic fracture; then, the rock specimen may be destroyed along the fracture plane.

In Table 3, when the rock specimen has a small dip angle (i.e., 10°, 20°, and 30°) of the preset fracture plane, its failure process is similar to that of the intact rock specimen. At the initial loading stage, with the compacting of the structure plane having a certain width, prominent instability units only occur in the upper part of rock and near the weak plane, while the lower part of rock has no instability units. With continuous loading, the failure process is same as that of the intact specimen. This indicates that the interface

**Table 2** Loading test of intact rock.

| Specimen             | Failure process   |   |   |  |   |
|----------------------|---|---|---|--|---|
| Intact rock specimen |  |  |  |  |  |
|                      | Step 20   | Step 31   | Step 37   | Step 40  | Step 45   |

**Table 3** Loading tests of rock with small dip angle structure planes (10°, 20°, and 30°).

| Specimens                                   | Failure process   |   |  |   |   |  |
|---|---|---|--|---|---|--|
| Rock specimen with a structure plane of 10° |  |  |  |  |  |  |
|   | Step 20   | Step 32   | Step 38  | Step 42   | Step 45   |  |
|   | Rock specimen with a structure plane of 20°                                       |  |   |   |  |   |
|   |   | Step 20   | Step 31  | Step 37   | Step 41   | Step 50  |
|   |   | Rock specimen with a structure plane of 30°                                       |  |   |  |  |
| Step 22                                     |   |   | Step 34  | Step 38   | Step 42   | Step 46  |

slipping effect of rock specimen with small dip angle structure planes is not obvious.

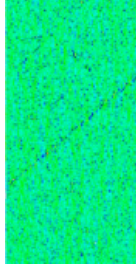
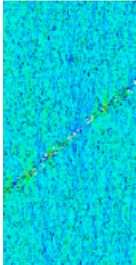
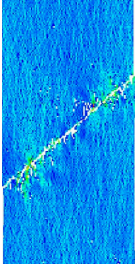
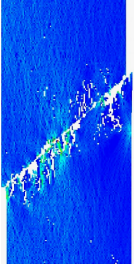
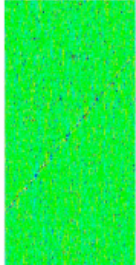
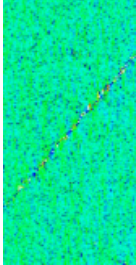
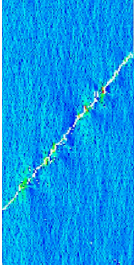
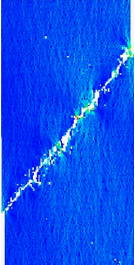
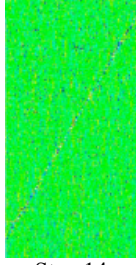
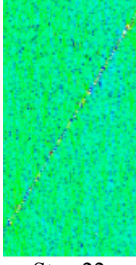
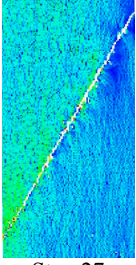
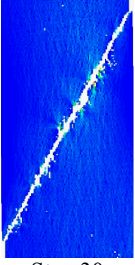
As shown in Table 4, when the rock specimen has a medium dip angle (i.e., 40°, 50°, and 60°) of the preset fracture plane, the failure of the rock block does not occur anymore on both sides of the plane, but it is prominently slipping along the plane. For instance, when the rock specimen has a structure plane with dip angle of 50°, at the 16th step, many instability units occur near the weak plane and in the upper part of rock. At the 25th step, instability units rise notably and the microfracture plane at the preset plane is formed; however, microcracks are not formed in the two sides of the rock. At the 28th step, the cracks at the preset plane extend into a macrofracture plane, and the macrocracks still not occur in the two sides of the rock. At the 35th step, slipping failure of rock specimen occurs along the macro failure plane at the preset plane. This indicates that the interface slipping effect of rock specimen with medium dip angle structure planes is notable. Moreover, as the dip angle of the structure plane increases, the slipping failure occurs more easily (i.e., loading steps are 45, 35, and 30 in turn), which shows that the slipping effect is enhanced with the dip angle of structure planes increasing.

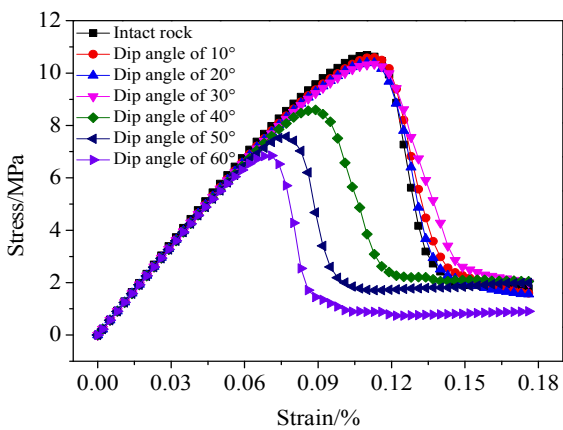
### 3.2.2. STRESS-STRAIN CHARACTERISTIC OF ROCK MASS WITH DIFFERENT DIP ANGLE STRUCTURE PLANES

As shown in Figure 6, at the initial loading stage, rock specimens with different dip angles are compacted, and the stress-strain curves coincide, showing a high degree of consistency. When the peak load is reached, the peak stress of intact rock specimen is 10.69 MPa, while that of with small dip angle structure planes (that is less than 30°) is in the range of 10.35–10.60 MPa. Moreover, the loading steps with the rock failure have little difference, which indicates that the small dip angle structure planes has little effect on the strength of rock specimens. With the rise in the dip angle of structure plane, the slipping effect of the plane gradually increases, and the strength of the rock specimen is significantly reduced. For instance, the peak stress with a dip angle of 40° is 8.60 MPa, which is much less than that of a dip angle of 30° (i.e., 10.35 MPa); moreover, with the rising dip angle, the failure strength of the rock specimen with 50° and 60° is 7.58 MPa and 6.85 MPa, respectively.

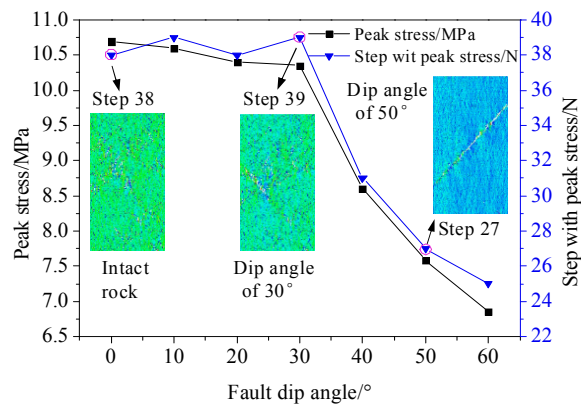
As the dip angle of the structure plane increases, the total strain prior to the peak stress decreases, and the total strain energy decreases, resulting in the reduction of bursting liability caused by internal

**Table 4** Loading tests of rock with medium dip angle structure planes (40°, 50°, and 60°).

| Specimens                                   | Failure process  |  |   |  |
|---|--|--|---|--|
| Rock specimen with a structure plane of 40° |   |   |   |   |
|   | Step 22  | Step 30  | Step 35   | Step 45  |
| Rock specimen with a structure plane of 50° |   |   |   |   |
|   | Step 16  | Step 25  | Step 28   | Step 35  |
| Rock specimen with a structure plane of 60° |  |  |  |  |
|   | Step 14  | Step 22  | Step 27   | Step 30  |



(a) Variation of stress-strain



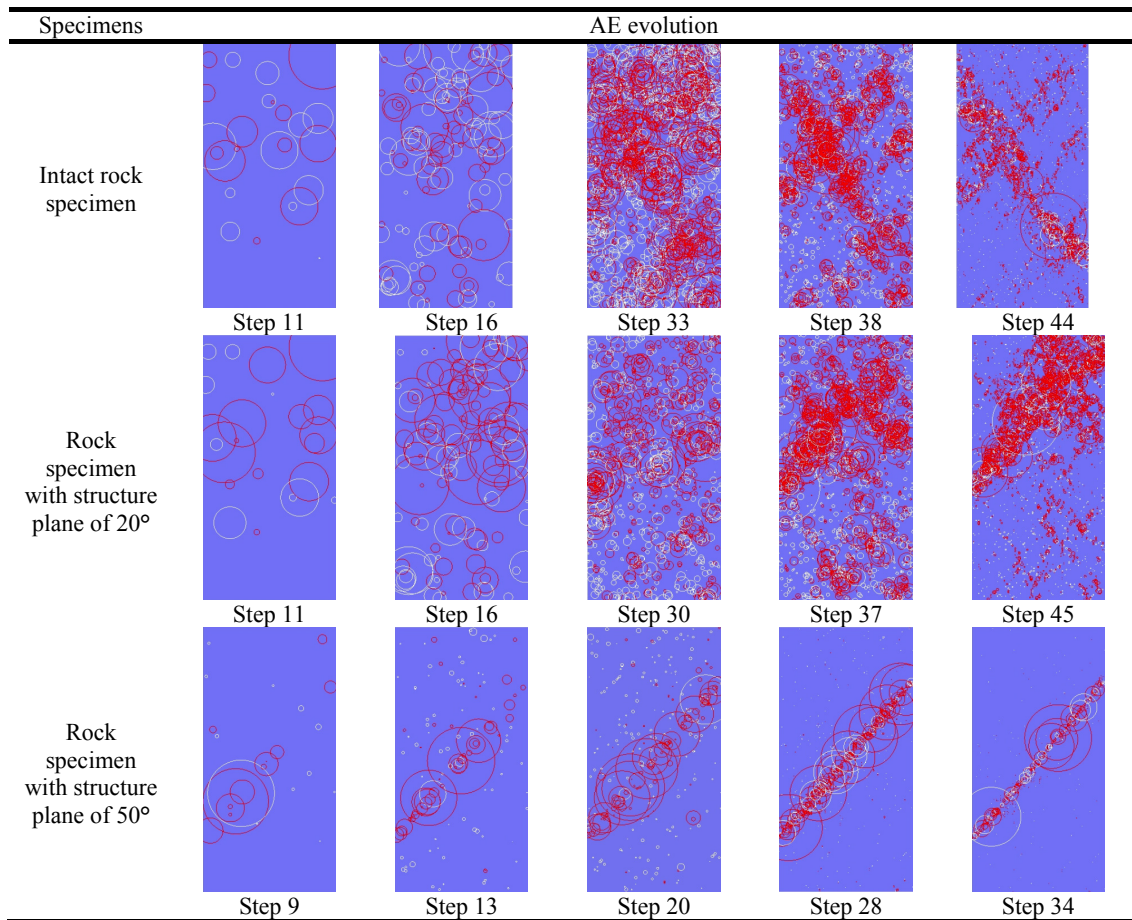
(b) Peak stress and its corresponding loading step

**Fig. 6** Variation curves of stress–strain with different dip angle of structural plane.

destruction of rock specimen. After the point of peak stress, softening characteristics of the stress–strain for rock specimen with medium dip angle structure plane are noticeable, and the slipping effect along the plane is obvious; this indicates that the strain energy accumulated prior to the peak stress does not completely act on the rock mass, but it is also released

through the structure plane. Hence, the bursting liability of rock specimen decreases with the rising of the dip angle of the structure plane, but the possibility of slipping instability along the plane increases.

Hence, the rock mass with different dip angle structure planes loading displays notable strength effect and interface slipping effect. The small dip

**Table 5** AE Evolution of typical rock specimens.

angle structure plane has little effect on the rock strength, and the interface slipping effect is not obvious, which mainly manifests as failure in the interior of rock. Meanwhile, the rock strength with medium dip angle structure plane is decreased prominently, and the interface slipping effect is notable, which is easy to slip along the structure plane; moreover, the strength weakening effect and the interface slipping effect are more obvious with the increasing of dip angle. The result agrees with the analysis results of the relationship between the fault slipping and fault dip angle with  $\sigma_3 = 0$  MPa in Section 2.

### 3.2.3. AE GENERATION OF ROCK MASS WITH DIFFERENT DIP ANGLE STRUCTURE PLANES

As a typical brittle material, rock can accumulate a large amount of elastic strain energy before failure, and this energy will be released in elastic wave mode and will create AE signals when the rock is destroyed. According to the aforementioned analysis, typical rock specimens, including an intact rock specimen, a rock specimen with small dip angle structure plane (20°), and a rock specimen with medium dip angle structure plane (50°), are chosen, and then the

temporal-spatial distribution and evolution of AE signals are obtained, as shown in Table 5. Among them, the circle diameter represents the AE intensity, the white circles are the AE signals generated by the compression shear failure, and the red circles are the AE signals produced by the tensile failure (Zhang and Li, 2017).

As shown in Table 5, when the rock specimen has a structure plane with dip angle of 20°, at the 11th step, many AE signals occur randomly in the upper part of the rock specimen while only a few of them in the lower part; at the 16th step, AE signals increase obviously and spread in the whole rock, but they are still randomly distributed; at the 30th step, the AE signals begin to develop orderly, and multiple AE accumulating points occur in the upper part of rock. Then, AE accumulation is more obvious at 37 steps, which indicates large amount strain energy releases; at the 45th step, the AE signals are mainly accumulated near the fracture plane caused by cracks interconnection, and the rock specimen undergoes failure. As to the rock specimen having a structure plane with dip angle of 50°, at the 9th step, many AE signals accumulate on the local structure plane, forming a AE accumulating zone at 13 steps; at the

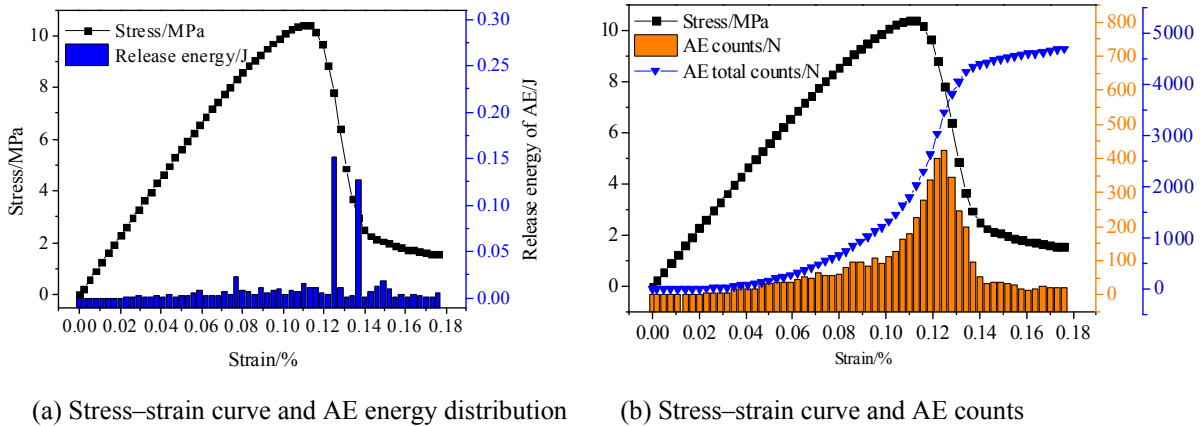


Fig. 7 AE characteristics of the rock specimen with a structure plane of 20°.

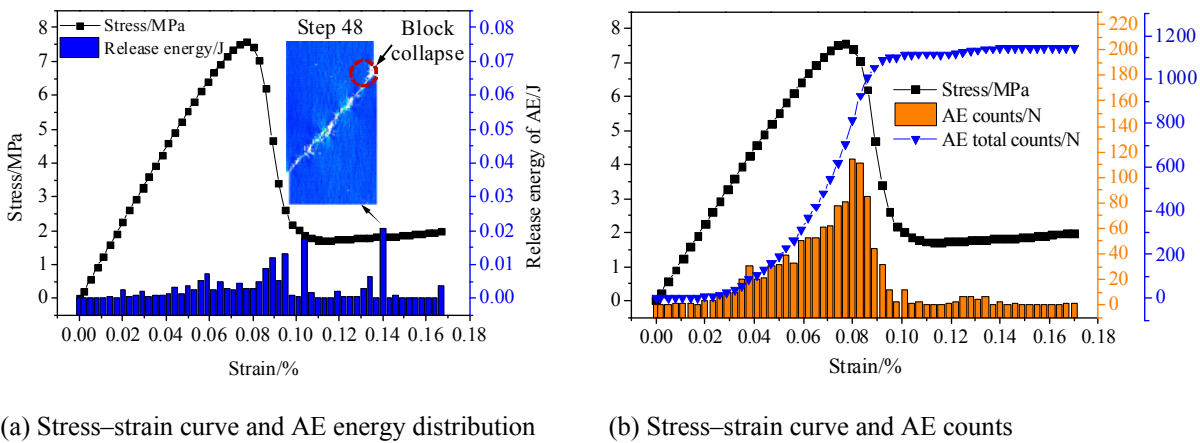


Fig. 8 AE characteristics of rock specimen with a structure plane of 50°.

28th step, AE signals are mainly accumulated near the preset structure plane, and the counts and energy of AE are still small in both sides of preset plane.

3.2.4. AE CHARACTERISTICS OF ROCK MASS WITH DIFFERENT DIP ANGLE STRUCTURE PLANES

Several parameters, including the counts, the cumulative counts and the release energy of AE signals, are used to describe the characteristic of AE. Figures 7 and 8 show the AE characteristics of rock loading with dip angle structure planes of 20° and 50°. Through analysis of the spatial-temporal distribution, the counts and energy release intensity of AE during rock failure, and the damage characteristics of rock mass with different dip angle structure planes, are studied.

However, as shown in Figures 7 and 8, when the rock specimen has a small dip angle or a medium dip angle structure plane, the counts and release energy of AE have notable stage characteristics with the loading on the rock. Prior to the peak stress, the rock specimen is in compaction stage and elastic stage, and the AE counts and release energy are small; hence, the AE counts and the release energy rise slowly at these stages, which indicates that the rock damage is small.

Near the peak stress point, the AE signals are active, and the counts are larger, which indicates that microcracks occur in the interior of rock. After reaching peak stress, the microcracks inside the rock converge and form macro fracture plane, thereby resulting in the stress decreasing and the elastic strain energy being released rapidly; hence, the AE counts and total counts rapidly rise to the peak values. Then, with the stress adjustment, AE counts are small, the total counts tend to be stable, and the release energy is less. However, it should be noted that for the rock with the dip angle structure plane of 50°, at 48 steps the release energy of AE increases rapidly, which may be caused by the collapse of the rock mass at the right side of the structure, thereby raising the bursting liability.

Figure 9 shows the maximum energy, total energy and total counts of AE signals from rock loading with different dip angle structure planes. Regardless of the maximum energy, total energy or total counts of AE signals, these three values are much higher in small dip angle structure planes than in medium dip angle structure planes; moreover, these three parameters drop with the dip angle of the plane increasing. For instance, the maximum AE energy of



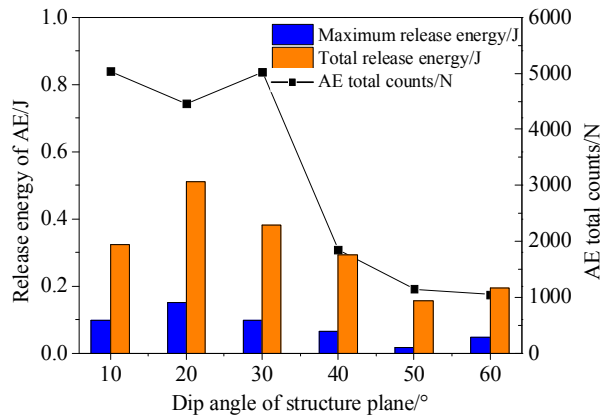


**Fig. 9** Energy and total counts of AE with different dip angle structure plane.

rock with small dip angle structure plane is in the range of 0.097 J–0.152 J, while that of with medium dip angle structure plane falls within 0.017 J–0.065 J. The total AE count number of rock with small dip angle structure plane is about 5000, while that of with medium dip angle structure plane is 1044–1850, much less than the former. Hence, it can be concluded that rock burst caused by internal failure with small dip angle structure plane is much more serious than that of with medium dip angle structure plane, where the rock easily slips along the preset plane.

#### 4. CONCLUSIONS

In this study, using mechanical analysis and numerical simulation, the strength weakening and interface slipping effects of rock masses with different dip angle structure planes are studied and revealed. We can obtain several conclusions as follows.

- The rock with a different dip angle structure plane shows a significant strength effect. The strength of rock with small dip angle structure plane is almost the same as that of intact rock, which indicates that the small dip angle structure has little effect on rock strength; on the other hand, the strength of rock with medium dip angle structure drops notably, and the strength weakening effect is more significant with a rising dip angle.
- The rock with a different dip angle structure plane shows a notable interface slipping effect. The interface slipping effect of rock with small dip angle structure is not obvious, and mainly manifests as failure inside the rock; meanwhile, the effect for a medium dip angle structure is notable and will be enhance with the dip angle rising, which is easy to slip along the structure plane.
- The bursting liability of rock with different dip angle structure planes is different. Compared to

the rock with small dip angle structure plane, the rock with medium dip angle structural plane is more easily to be broken and its failure steps are less; however, the release total energy and total AE counts are smaller, which indicates that the rock burst caused by rock failure may be less serious.

Studying the micromechanical behaviors of rock mass with a structure plane can provide the basis for the precursory characteristics of macro-fracture and lay a solid foundation for the study of the rock bursts near faults.

#### ACKNOWLEDGMENTS

The study was funded by the National Natural Science Foundation of China (nos. 51574155, 51504145, 51804182, and 51704182), Natural Science Foundation of Shandong Province (no. ZR2017BEE050), Scientific Research Foundation of Shandong University of Science and Technology for Recruited Talents (no. 2015RCJJ057), Shandong Provincial Key R & D Plan (Public Welfare Special Program) of China (no. 2017GGX20125), and Shandong Provincial Institute of Science and Technology Plan (no. J17KB041).

#### REFERENCES

- Bahaaddini, M.: 2017, Effect of boundary condition on the shear behaviour of rock joints in the direct shear test. *Rock Mech. Rock Eng.*, 50, 5, 1141–1155. DOI: 10.1007/s00603-016-1157-z
- Bahaaddini, M, Hagan, P.C., Mitra, R. and Khosravi, M.H.: 2016, Experimental and numerical study of asperity degradation in the direct shear test. *Eng. Geol.*, 204, 41–52. DOI: 10.1016/j.enggeo.2016.01.018
- Cai, W.: 2015, Fault rockburst induced by static and dynamic loads superposition and its monitoring and warning, Ph.D. thesis, China University of Mining and Technology, Xuzhou, China, 20pp.
- Cao, P., Zhong, Y.F., Li, Y.J. and Liu, J.: 2015, Investigations on direct shear tests and PFC2D numerical simulations of rock-like materials with a hole and prefabricated cracks. *Key Eng. Mater.*, 627, 477–480. DOI: 10.4028/www.scientific.net/KEM.627.477
- Cao, R.H., Lin, H. and Cao, P.: 2018, Strength and failure characteristics of brittle jointed rock-like specimens under uniaxial compression: digital speckle technology and a particle mechanics approach. *Int. J. Min. Sci. Technol.*, 28, No. 4, 669–677. DOI: 10.1016/j.ijmst.2018.02.002
- Day, J.J., Diederichs, M.S. and Hutchinson, D.J.: 2017, New direct shear testing protocols and analyses for fractures and healed intrablock rockmass discontinuities. *Eng. Geol.*, 229, 53–72. DOI: 10.1016/j.enggeo.2017.08.027
- Feng, X.T., Zhang, X.W., Yang, C.X., Kong, R., Liu, X.Y. and Peng, S.: 2017, Evaluation and reduction of the end friction effect in true triaxial tests on hard rocks. *Int. J. Rock Mech. Min. Sci.*, 97, 144–148. DOI: 10.1016/j.ijrmms.2017.04.002
- Hubbert, M.K. and Rubey, W.W.: 1961, Role of fluid pressure in mechanics of overthrust faulting. *Geol.*

- Soc. Am. Bull., 70, 5, 115.  
DOI: 10.1130/0016-7606(1959)70[167:ROFPIM]2.0.CO;2
- Lee, S., Chang, I., Chung, M.K., Kim, Y.Y. and Kee, J.: 2017, Geotechnical shear behavior of Xanthan Gum biopolymer treated sand from direct shear testing. *Geomech. Eng.*, 12, 5, 831–847.  
DOI: 10.12989/gae.2017.12.5.831
- Jiang, J.Q., Wang, P., Jiang, J.S., Zheng, P.Q. and Feng, F.: 2018, Numerical simulation on mining effect influenced by a normal fault and its induced effect on rock burst. *Geomech. Eng.*, 14, 4, 337–344.  
DOI: 10.12989/gae.2018.14.4.337
- Jiang, L. S., Wang, P., Zhang, P.P., Zheng, P.P. and Xu, B.: 2017, Numerical analysis of the effects induced by normal faults and dip angles on rock bursts. *CR Mecanique*, 345, 10, 690–705.  
DOI: 10.1016/j.crme.2017.06.009
- Jiang, Y.D., Wang, T., Song, Y.M., Wang, X. and Zhang, W.: 2013, Experimental study on the stick-slip process of coal-rock composite samples. *J. China Coal Soc.*, 38, 2, 177–182.  
DOI : 10.13225/j.cnki.jccs.2013.02.013
- Kim, B.S., Kato, S., Park, S.W. and Takeshita, Y.: 2016, DEM simulation on opening between shear boxes in direct shear test. *Japanese Geotech. J.*, 11, 1, 21–31.  
DOI: <https://doi.org/10.3208/jgs.11.21>
- Ma, Y., Jing, H.W. and Chen, Y.H.: 2007, Numerical simulation of failure mechanism of surrounding rocks in mining induced roadway and its support. *J. Min. Saf. Eng.*, 24, 1, 109–113.
- Moayed, R.Z., Alibolandi, M. and Alizadeh, A.: 2016, Specimen size effects on direct shear test of silty sands. *Int. J. Geotech. Eng.*, 11, 2, 198–205.  
DOI: 10.1080/19386362.2016.1205166
- Sainoki, A. and Mitri, H.S.: 2014, Evaluation of fault-slip potential due to shearing of fault asperities. *Can. Geotech. J.*, 52, 10, 1417–1425.  
DOI: 10.1139/cgj-2014-0375
- Shen, M.R. and Chen, J.F.: 2006, *Rock mechanics*, Tongji University Press Shanghai, 78 pp.
- Tang, C.A., Wang, J.M. and Zhang, J.J.: 2010, Preliminary engineering application of microseismic monitoring technique to rockburst prediction in tunneling of Jinping II project. *Rock Mech. Geotech. Eng.*, 2, No. 3, 193–208.  
DOI: <https://doi.org/10.3724/SP.J.1235.2010.00193>
- Wang, P., Jiang, L. S., Jiang, J. Q., Zheng, P. Q. and Li, W.: 2018, Strata behaviors and rock burst-inducing mechanism under the coupling effect of a hard, thick stratum and a normal fault. *International Int. J. Geomech*, 18, No. 2, 04017135.  
DOI:10.1061/(ASCE)GM.1943-5622.0001044
- Wang, Y.J., Niu, H.P., and Duan, D.: 2017, RFPA2D numerical simulation of carbonaceous mudstone under uniaxial compression. *Coal Technology*, 36, No. 7, 50–51. DOI : 10.13301/j.cnki.ct.2017.07.019
- Wang, T.: 2012, Mechanism of coal bumps induced by fault reactivation. Ph.D. thesis, China University of Mining and Technology, Beijing, China.
- Zhao, S.K., Zhang, Y., Han, R.J., Jiang, H.B., Zhang, N.B. and Xu, Z.J.: 2013, Numerical simulation experiments on bursting liability evolution of compound coal-rock structure. *J. Liaoning Univ. Nat. Sci.*, 32, No. 11, 1441–1446.  
DOI: 10.3969/j.issn.1008-0562.2013.11.001
- Zhang, J.W. and Li, Y.L.: 2017, Ultrasonic vibrations and coal permeability: Laboratory experimental investigations and numerical simulations. *International Int. J. Min. Sci. Technol*, 27, No. 2, 221–228.  
DOI: <https://doi.org/10.1016/j.ijmst.2017.01.001>